A Color Image Watermarking Based on Tensor Analysis

HAIYONG XU, GANGYI JIANG, (Member, IEEE), MEI YU, AND TING LUO

College of Science and Technology, Ningbo University, Ningbo 315211, China
Faculty of Information Science and Engineering, Ningbo University, Ningbo 315211, China

Corresponding author: Mei Yu (yumei@nbu.edu.cn)

ABSTRACT Since most of the color image watermarking methods embed the watermark information in each channel or one channel of a color image, the redundant information of the color image cannot be sufficiently utilized, resulting in the poor ability to resist attacks. In this paper, a novel blind color image watermarking method based on the tensor domain is proposed, and it takes efficient account of the overall characteristics of color images and spreads the watermark information into three channels of color images based on tensor decomposition. Exploring the new tensor domain to embed and extract watermark information and the theoretical proof of the optimal embedding position of the core tensor are the major technical contributions of this paper. To be more specific, first, the RGB channels of the color image as a tensor are considered, and the tensor decomposition is used to obtain the core tensor. Then, based on the theoretical proof, the optimal embedding position of the core tensor is obtained, and the watermark information is embedded into the core tensor. Finally, the watermark information is spread to the three channels of the color image through the inverse tensor decomposition. The experimental results show that the proposed method has better invisibility and stronger robustness for the most common attacks.

INDEX TERMS Color image watermarking, tensor domain, tensor Decomposition.

I. INTRODUCTION

With the rapid development of the Internet and computer technology, image, video and other multimedia information storage, reproduction and dissemination has become very convenient [1], [2]. However, since images and videos are easy to modify and quickly spread, which leads to piracy, infringement and other acts becoming increasingly widespread, multimedia information security has attracted much attention [3]. Digital watermarking is now a relatively focused technique aimed at providing a reliable way to authenticate images or protect copyrights [4], [5].

As a new technology for the copyright protection of digital media, digital watermarking embeds copyright information (i.e., watermark information) into digital media. Usually, the watermark information is invisible and needs to be detected or extracted. In this way, the extracted watermark information is used to prove the copyright's attribution or the certification of the digital product in the copyright dispute, which effectively protects the copyright of the digital multimedia and improves its security [6]–[8]. Generally, the

watermarking methods have two basic characteristics: robustness and fidelity [9]. Therefore, a good watermarking method can effectively balance the relationship between its robustness and fidelity [10].

In recent years, image watermarking methods were divided into two types according to the embedding domain: the spatial domain-based watermarking method [11], [12] and the transform domain-based watermarking method [13]–[18]. For the spatial domain-based watermarking method, the basic idea is to directly modify the pixel values by using the redundancy of the spatial domain. Chan and Cheng [11] proposed a data hiding scheme using the simple Least-Significant Bit (LSB) substitution with an optimal pixel adjustment process. This method is easy to be implemented and does not generate serious distortions in the image; however, it is not very robust against attacks. To improve the spatial domain-based watermarking methods, some block-based methods were proposed instead of directly modifying the pixel method. Nasir *et al.* [12] proposed a multiple-watermarking method for the copyright protection

of color images, in which a binary watermark image is divided into four parts and embedded into different regions of the blue component of the color image in the spatial domain.

Compared with the spatial domain-based watermarking methods, the transform domain-based watermarking methods are more widely applied. For the transform domain-based watermarking methods, the watermarking information is embedded into the new domain by using various transformations, such as the discrete cosine transform (DCT), the discrete Fourier transform (DFT), the discrete wavelet transform (DWT), the discrete Laguerre transform (DLT) and the discrete Hadamard transform (DHT). Usman *et al.* [13] proposed a novel method of adaptive visual tuning of the watermark in the DCT domain. The method intelligently selects the appropriate frequency bands and the optimal strength of the alteration. Vahedi *et al.* [14] proposed a DWT-based watermarking method by considering the problem of logo watermarking and employing the genetic algorithm's optimization principles. He *et al.* [15] proposed a watermarking method based on DFT and Quantized index modulation (QIM). Because DFT methods have strong robustness to translation, rotation, and scaling, the phase information of the image does not change when the image is subjected to a geometric attack, which makes the methods have strong robustness to geometric attacks. In addition, other transform-based watermarking methods are proposed, such as the DCT combined with the just noticeable difference (JND) method [16], [17], the DWT-based method according to the JND threshold [18], and the DWT-based method that employs the characteristics of the human visual systems (HVS) [19].

As shown in the above discussion, most watermarking methods embed watermark information in grayscale images. Recently, many watermarking methods have focused on the color image. For color image watermarking methods, the color space is usually transformed first, and then, the watermark information is embedded in the luminance component or in each channel of the color image. Barni *et al.* [20] proposed the DCT-based color image watermarking method by exploiting the HVS's characteristics and the correlation between RGB channels in order to achieve a good trade-off between robustness and imperceptibility. Ahmidi and Safabakhsh [17] proposed a DCT-based color image watermarking method that uses the sensitivity of human eyes to adaptively embed watermarks into color images. Su *et al.* [21] proposed embedding the watermark into the direct current (DC) coefficients in the spatial domain rather than the DCT domain, which is simple and efficient. Regarding DWT-based color image watermarking, Al-Otum *et al.* [22] proposed a color image watermarking method that performs a DWT on the three color channels in order to construct a wavelet-tree and then searches for robust bit host locations based on dominant relations. Chou *et al.* [23] proposed a color image watermarking method to hide watermarks in most distortion-tolerable signals within the three color channels of the host image without resulting in perceivable distortion. Similarly, the DFT

has been extensively studied in color image watermarking schemes. Tsui *et al.* [24] proposed a color image method that represents the host image in the $La*b*$ color space and encoded the chromatic channels a* and b* into complex numbers $a + jb$. The watermark was then embedded in the frequency domain by using the spatio chromatic DFT. In addition, researchers have been widely concerned with the quaternion discrete Fourier transform (QDFT), which offers an effective way to jointly address the three channels of the color image by spreading the watermark information into the three channels [25]–[27]. Tsui *et al.* [25] proposed a QDFT-based color image watermarking method in the $La*b*$ color space. Recently, Chen *et al.* [26] proposed a color image watermarking method based on the 4D-QDFT and QIM. On this basis, Ouyang *et al.* [27] proposed a blind color image watermarking scheme based on the QDFT and an improved uniform log-polar mapping.

From the above discussion, most of color image watermarking methods have been proposed to embed a watermark in each channel or one channel of the color image. The redundant information of the color image is not fully utilized, which may result in a poor ability to resist attacks. Therefore, this paper explores a novel color image watermarking method in the tensor domain, and it takes efficient account of the overall characteristics of color images and spreads the watermark information into three channels of color images based on tensor decomposition. The main contributions of the present study as follows:

(1) The color image is regarded as a tensor, which brings many benefits to the watermarking embedding and extraction process.

(2) The optimal embedding position is determined by theoretical analysis in tensor domain.

(3) The tensor decomposition can diffuse the watermark information to the three channels of the color channel and effectively achieve the robust performance of the watermarking method.

The rest of the paper is organized as follows. In Section II, some definitions and theoretical analyses of the tensor domain are described. The proposed color image watermarking method is reported in Section III. Experiments to test its robustness are carried out and discussed in Section IV. Finally, Section V concludes the paper.

II. TENSOR DOMAIN: FROM MATRIX TO TENSOR
In this section, we describe the basic definitions of the tensor, the motivation of the paper, and the theoretical analysis of watermark embedding in the tensor domain.

A. NOTATIONS AND DEFINITIONS
We first denote scalars as small letters (a, b, etc.), vectors as bold small letters ($\mathbf{a}$, $\mathbf{b}$, etc.), matrices as bold capital letters ($\mathbf{A}$, $\mathbf{B}$, etc.), and higher order tensors as calligraphic letters ($\mathcal{A}$, $\mathcal{B}$, etc.).

Image/video data present more dimensionality with the development of big data. The traditional data representation

often transforms high-dimensional data into vectors. However, this processing often leads to two problems. First, vectorization leads to high dimensionality and forms the dimensionality disaster; second, vectorization destroys the structural information of data. The tensor is a multidimensional data form (in fact, the tensor is a high-order generalization of vectors and matrices), which can overcome these two problems well.

A *p*th-order tensor is denoted $\mathcal{A} \in R^{I_1 \times I_2 \times \cdots \times I_p}$ where $I_1, I_2, \cdots, I_p \in Z$ indicates the number of elements for each dimension. The elements of $\mathcal{A}$ are denoted $a_{i_1 \cdots i_n \cdots i_p}$, where $1 \leq i_n \leq I_n, n = 1, \cdots, p$. For example, a color image can be considered a tensor of order 3, with $I_1 = n$, $I_2 = m$, and $I_3 = 3$, if it is composed by 3 channels of the dimension $n \times m$ pixels.

Higher order tensors can also be represented by sets of matrices. For a third-order tensor, the horizontal, lateral, and frontal slides can be formed and denoted by $A_{i::}$, $A_{:j:}$ and $A_{::k}$, respectively.

Next, we will define the basic algebraic operation of the tensor, including the inner product of the tensor and the n-mode product of the tensor.

Definition 1: The inner product $\langle \mathcal{A}, \mathcal{B} \rangle$ of two same-sized tensors, $\mathcal{A}$, $\mathcal{B}$, is defined as follows:

$$\langle \mathcal{A}, \mathcal{B} \rangle = \sum_{i_1} \sum_{i_2} \cdots \sum_{i_p} a_{i_1 i_2 \cdots i_p} b_{i_1 i_2 \cdots i_p} \quad (1)$$

Then, according to the inner product of the tensor, the tensor's Frobenius norm can be defined as follow.

Definition 2: The Frobenius-norm of a tensor $\mathcal{A}$ is given by

$$\|\mathcal{A}\|_F = \sqrt{\langle \mathcal{A}, \mathcal{A} \rangle} = \left(\sum_{i_1} \sum_{i_2} \sum_{i_p} |a_{i_1 i_2 \cdots i_p}|^2 \right)^{1/2} \quad (2)$$

The tensor can also be multiplied by the matrix, which is more complex than the multiplication between matrices. The n-mode product of the tensor can be defined as follows.

Definition 3: The n-mode product of an Nth-order tensor $\mathcal{A} \in R^{I_1 \times I_2 \times \cdots I_n \times \cdots \times I_p}$ by a matrix $\mathbf{U} \in R^{J_n \times I_n}$, which is denoted by $\mathcal{A} \times_n \mathbf{U}$, is an $(I_1 \times I_2 \times \cdots \times I_{n-1} \times J_n \times I_{n+1} \times \cdots \times I_p)$ -tensor of which the entries are given by

$$(\mathcal{A} \times_n \mathbf{U})_{i_1 \times i_2 \times \cdots \times i_{n-1} \times j_n \times i_{n+1} \times \cdots \times i_p}$$
$$= \sum_{i_n} a_{i_1 \times i_2 \times \cdots \times i_{n-1} \times i_n \times i_{n+1} \times \cdots \times i_p} u_{j_n i_n} \quad (3)$$

B. TENSOR DECOMPOSITION: FROM SVD TO TENSOR DECOMPOSITION

To define tensor decomposition, we first introduce the singular value decomposition (SVD), which is the most famous method of matrix decomposition.

Given matrix $\mathbf{D} \in R^{I_1 \times I_2}$, it can be decomposed by the SVD as follows:

$$\mathbf{D} = \mathbf{U}_1 \boldsymbol{\Sigma} U_2^T \quad (4)$$

where $\mathbf{U}_1$ denotes a left matrix, $\mathbf{U}_2$ represents a right matrix, and $\boldsymbol{\Sigma}$ is a diagonal matrix. In fact, the matrix can be seen as a second-order tensor, and then, the SVD decomposition can be rewritten as follows:

$$\mathbf{D} = \boldsymbol{\Sigma} \times_1 \mathbf{U}_1 \times_2 \mathbf{U}_2 \quad (5)$$

For higher-order ($p > 2$) tensor decomposition, there are two categories: one is CANDECOMP/PARAFAC decomposition (CP) decomposition, and the other is Tucker decomposition. Here, we focus on the Tucker decomposition.

Given a *p*-order tensor $\mathcal{A} \in R^{I_1 \times I_2 \times \cdots \times I_p}$, we seek a Tucker model, as defined below, to approximate the tensor $\mathcal{A}$ as

$$\mathcal{A} \approx \mathcal{G} \times_1 \mathbf{U}_1 \times_2 \cdots \times_p \mathbf{U}_p \quad (6)$$

Then, the optimization problem to be solved is

$$\min_{\mathcal{G}, \mathbf{U}_1, \cdots, \mathbf{U}_p} \left\| \mathcal{A} - \mathcal{G} \times_1 \mathbf{U}_1 \times_2 \cdots \times_p \mathbf{U}_p \right\|$$
$$\text{subject to } \mathcal{G} \in R^{J_1 \times J_2 \times \cdots \times J_p}$$
$$\mathbf{U}_n \in R^{I_n \times J_n} \text{ and columnwise orthogonal}$$
$$\text{for } n = 1, \cdots, p. \quad (7)$$

where $\mathcal{G}$ is a *p*-order tensor of dimension $J_1 \times J_2 \times \cdots \times J_p$, which is called the core tensor, and $\mathbf{U}_n \in R^{I_n \times J_n}$ is the matrix applied along the *n*-mode. Note that unlike the singular value matrix in the SVD decomposition, the core tensor $\mathcal{G}$ does not take the diagonal structure, which is generally a full tensor. That is, its non-diagonal elements are usually not equal to zero.

We use the following Tucker3 algorithm to perform the calculation.

1) For $i = 1, 2, \cdots, p$, we use the standard SVD to calculate the unfolding matrix in each dimension from $\mathcal{A}$: $\mathbf{A}_{(i)} = \mathbf{U} \boldsymbol{\Sigma} \mathbf{V}^T$. The orthogonal matrix $\mathbf{U}_i$ is defined as $\mathbf{U}_i = \mathbf{U}$, which is the left matrix of the SVD.

2) We use the inverse of the tensor product to calculate the core tensor:

$$\mathcal{G} = \mathcal{A} \times_1 \mathbf{U}_1^T \times_2 \cdots \times_p \mathbf{U}_p^T \quad (8)$$

Since $\mathbf{U}\mathbf{U}_i^T = \mathbf{U}_i^T\mathbf{U} = \mathbf{I}$, the core tensor $\mathcal{G}$ in Eq. (8) is calculated by $\mathbf{U}_i^T$. In this paper, the core tensor is used to embed and extract the watermarking information.

C. THEORETICAL ANALYSIS OF TENSOR DOMAIN-BASED COLOR IMAGE WATERMARKING

Recently, most of the digital color image watermarking methods have tended to consider the three channels separately. Here, the three channels of the color image are considered as a whole. This inspires us to consider the color image as a tensor rather than a matrix or a vector.

After the color image is treated as a tensor, it is natural that the problem is where the watermark is embedded in the tensor domain. To answer this question, we give the following theoretical analysis.

Property 1: If $\mathbf{Q}$ is a standard orthogonal matrix, then $\|\mathcal{A} \times_n \mathbf{Q}\| = \|\mathcal{A}\|$.

Theorem 1: Given two tensors $\mathcal{A}, \mathcal{B} \in R^{I_1 \times I_2 \times \cdots \times I_p}$, assuming that the Tucker decomposition of the two tensors $\mathcal{A}, \mathcal{B}$ has the same projection orthogonal matrix, which is $\mathcal{A} = \mathcal{G}_A \times_1 \mathbf{U}_1 \times_2 \cdots \times_p \mathbf{U}_p$, $\mathcal{B} = \mathcal{G}_B \times_1 \mathbf{U}_1 \times_2 \cdots \times_p \mathbf{U}_p$, then $\|\mathcal{A} - \mathcal{B}\|^2 = \|\mathcal{G}_A - \mathcal{G}_B\|^2$.

Proof: We have the following:

$$\|\mathcal{A} - \mathcal{B}\|^2 = \langle \mathcal{A} - \mathcal{B}, \mathcal{A} - \mathcal{B} \rangle = \langle \mathcal{A}, \mathcal{A} \rangle - 2\langle \mathcal{A}, \mathcal{B} \rangle + \langle \mathcal{B}, \mathcal{B} \rangle$$
$$= \|\mathcal{A}\|^2 - 2\langle \mathcal{A}, \mathcal{B} \rangle + \|\mathcal{B}\|^2 \qquad (9)$$

Then, with *property* 1, we have $\|\mathcal{A}\|^2 = \|\mathcal{G}_A\|^2$ and $\|\mathcal{B}\|^2 = \|\mathcal{G}_B\|^2$.

According to the definition of the inner product and the orthogonality of projection matrix, we have

$$\langle \mathcal{A}, \mathcal{B} \rangle = \langle \mathcal{G}_A, \mathcal{G}_B \rangle = \sum_{i_1} \sum_{i_2} \cdots \sum_{i_p} g^A_{i_1 i_2 \cdots i_p} \cdot g^B_{i_1 i_2 \cdots i_p} \qquad (10)$$

Thus,

$$\|\mathcal{A} - \mathcal{B}\|^2$$
$$= \|\mathcal{A}\|^2 - 2\langle \mathcal{A}, \mathcal{B} \rangle + \|\mathcal{B}\|^2$$
$$= \sum_{i_1} \sum_{i_2} \cdots \sum_{i_p} (g^A_{i_1 i_2 \cdots i_p})^2 - 2 \sum_{i_1} \sum_{i_2} \cdots \sum_{i_p} g^A_{i_1 i_2 \cdots i_p}$$
$$\cdot g^B_{i_1 i_2 \cdots i_p} + \sum_{i_1} \sum_{i_2} \cdots \sum_{i_p} (g^B_{i_1 i_2 \cdots i_p})^2$$
$$= \sum_{i_1} \sum_{i_2} \cdots \sum_{i_p} \left(g^A_{i_1 i_2 \cdots i_p} - g^B_{i_1 i_2 \cdots i_p} \right)^2 = \|\mathcal{G}_A - \mathcal{G}_B\|^2$$
$$(11)$$

$\square$

From *Theorem* 1, the squared error sum for the two tensors $\mathcal{A}$ and $\mathcal{B}$ is equal to the squared error sum between the two core tensors $\mathcal{G}_\mathcal{A}$ and $\mathcal{G}_\mathcal{B}$. When $\mathcal{G}_\mathcal{A}$ and $\mathcal{G}_\mathcal{B}$ simply have a little difference, the value of $\|\mathcal{A} - \mathcal{B}\|^2$ is close to zero. It means that the two tensors $\mathcal{A}$ and $\mathcal{B}$ are nearly identical. If the two tensors $\mathcal{A}$ and $\mathcal{B}$ are regarded as the host color image and the watermarked color image, we can embed the watermark information in the core tensor subspace when designing the watermarking method. Thus, the difference between the host color image and the watermarked color image is as small as possible.

After we have decided to embed the watermark information into the core tensor subspace, it is natural that the problem is where the core tensor is embedded in the watermark, thus making the original space change the smallest. To answer this problem, the following theorem is proposed to illustrate the optimal embedding position of the watermark information.

Theorem 2: Given any p-order tensor $\mathcal{A} \in R^{I_1 \times I_2 \times \cdots \times I_p}$, its Tucker decomposition is $\mathcal{A} \approx \mathcal{G} \times_1 \mathbf{U}_1 \times_2 \cdots \times_p \mathbf{U}_p$. Then, we have $|g_{11\cdots1}| = \max\{ |g_{i_1 i_2 \cdots i_p}| \mid 1 \leq i_n \leq I_n \}$ in the core tensor $\mathcal{G}$.

Proof: A matrix representation of the Tucker 3 decomposition can be obtained by unfolding $\mathcal{A} \in R^{I_1 \times I_2 \times \cdots \times I_p}$ and

the core tensor $\mathcal{G}$ in Eq. (8):

$$\mathbf{A}_{(n)} = \mathbf{U}_n \cdot \mathbf{G}_{(n)} \cdot \left(\mathbf{U}_{n+1} \otimes \mathbf{U}_{n+2} \otimes \cdots \otimes \mathbf{U}_p \otimes \mathbf{U}_1 \otimes \mathbf{U}_2 \right.$$
$$\left. \otimes \cdots \otimes \mathbf{U}_{n-1} \right)^T \quad (12)$$

where $\mathbf{A}_{(n)}$ and $\mathbf{G}_{(n)}$ are the mode-n matricization of tensors $\mathcal{A} \in R^{I_1 \times I_2 \times \cdots \times I_p}$ and $\mathcal{G}$, respectively. The symbol $\otimes$ denotes the Kronecker Product [28], [29]. The Kronecker product of two matrices $\mathbf{F} \in R^{I_1 \times I_2}$ and $\mathbf{G} \in R^{J_1 \times J_2}$ is defined according to

$$\mathbf{F} \otimes \mathbf{G} = (f_{i_1 i_2} \mathbf{G})_{1 \leq i_1 \leq I_1; 1 \leq i_2 \leq I_2} \qquad (13)$$

and $\mathbf{U}_1, \mathbf{U}_2, \cdots, \mathbf{U}_p$ are orthogonal matrices.

Now consider the case in Eq. (12) where $\mathbf{U}_n$ is obtained from the SVD of $\mathbf{A}_{(n)}$ as

$$\mathbf{A}_{(n)} = \mathbf{U}_n \cdot \mathbf{\Sigma}_n \cdot \mathbf{V}_n^T \qquad (14)$$

In it, $\mathbf{V}_n$ is orthogonal and $\mathbf{\Sigma}_n = \mathrm{diag}(\sigma_1^{(n)}, \sigma_2^{(n)}, \cdots, \sigma_{I_n}^{(n)})$, where

$$\sigma_1^{(n)} \geq \sigma_2^{(n)} \geq \cdots \geq \sigma_{I_n}^{(n)} \geq 0 \qquad (15)$$

Taking into account the Kronecker factor in Eq. (13), the comparison of Eqs. (12) and (14) shows that

$$\mathbf{U}_n \cdot \mathbf{G}_{(n)} \cdot \left(\mathbf{U}_{n+1} \otimes \mathbf{U}_{n+2} \otimes \cdots \otimes \mathbf{U}_p \otimes \mathbf{U}_1 \otimes \mathbf{U}_2 \right.$$
$$\left. \otimes \cdots \otimes \mathbf{U}_{n-1} \right)^T = \mathbf{U}_n \cdot \mathbf{\Sigma}_n \cdot \mathbf{V}_n^T \quad (16)$$

The term $\mathbf{U}_{n+1} \otimes \mathbf{U}_{n+2} \otimes \cdots \otimes \mathbf{U}_p \otimes \mathbf{U}_1 \otimes \mathbf{U}_2 \otimes \cdots \otimes \mathbf{U}_{n-1}$ is defined as follows:

$$\mathbf{U}_{n+1} \otimes \mathbf{U}_{n+2} \otimes \cdots \otimes \mathbf{U}_p \otimes \mathbf{U}_1 \otimes \mathbf{U}_2 \otimes \cdots \otimes \mathbf{U}_{n-1} = \mathbf{W}_n$$
$$(17)$$

Due to the orthogonality of $\mathbf{U}_n$, Eq. (16) can be rewritten as

$$\mathbf{G}_{(n)} \cdot \mathbf{W}_n^T = \mathbf{\Sigma}_n \cdot \mathbf{V}_n^T \qquad (18)$$

and

$$\mathbf{G}_{(n)} = \mathbf{\Sigma}_n \cdot \mathbf{V}_n^T \cdot \mathbf{W}_n \qquad (19)$$
$$\mathbf{\Sigma}_n = \mathbf{G}_{(n)} \cdot (\mathbf{W}_n)^T \cdot \mathbf{V}_n \qquad (20)$$

Then,

$$\langle \mathbf{\Sigma}_n, \mathbf{\Sigma}_n \rangle = \left\langle \mathbf{G}_{(n)} \cdot (\mathbf{W}_n)^T \cdot \mathbf{V}_n, \mathbf{G}_{(n)} \cdot (\mathbf{W}_n)^T \cdot \mathbf{V}_n \right\rangle$$
$$= \mathbf{G}_{(n)} \cdot (\mathbf{W}_n)^T \cdot \mathbf{V}_n \cdot \mathbf{V}_n^T \cdot \mathbf{W}_n \cdot (\mathbf{G}_{(n)})^T$$
$$= \langle \mathbf{G}_{(n)}, \mathbf{G}_{(n)} \rangle \qquad (21)$$

Since $\mathbf{\Sigma}_n = \mathrm{diag}(\sigma_1^{(n)}, \sigma_2^{(n)}, \cdots, \sigma_{I_n}^{(n)})$, $\mathbf{G}_{(n)}$ has mutually orthogonal rows. That is,

$$\langle g_{i_n = \alpha}, g_{i_n = \beta} \rangle = 0 \quad \text{when } \alpha \neq \beta, \qquad (22)$$

and

$$\|g_{i_n = 1}\| = \sigma_1^{(n)} \geq \|g_{i_n = 2}\| = \sigma_2^{(n)} \geq \cdots \geq \|g_{i_n = I_n}\|$$
$$= \sigma_{I_n}^{(n)} \geq 0. \qquad (23)$$

From Eq. (23), $\|g_{i_n=1}\|$ obtains the maximum value for one of $n \in \{1, 2, \cdots, p\}$.

For the all matrices $\mathbf{G}_{(n)}$, $g_{11\cdots1}$ always appears in $g_{i_n=1}$. To ensure that $\|g_{i_n=1}\|$ is the maximum value of a certain value of n, $|g_{11\cdots1}|$ takes the maximum value in the absolute value of the elements of the core tensor. That is,

$$|g_{11\cdots1}| = \max\{|g_{i_1 i_2 \cdots i_p}| \mid 1 \le i_n \le I_n\} \qquad (24)$$

$\square$

We can also give an example to verify *Theorem* 2 from a computational point of view.

Example: Consider the randomly generated $(3 \times 3 \times 3)$ tensor $\mathcal{A}$ defined by a matrix unfolding $\mathbf{A}_{(1)}$, which is equal to matrix as shown at the bottom of this page.

The 1-mode singular vectors are the columns of the left singular matrix of $\mathbf{A}_{(1)}$. In the same way, $\mathbf{U}_2$ and $\mathbf{U}_3$ can be obtained with

$$\mathbf{U}_1 = \begin{pmatrix} -0.4026 & -0.8029 & 0.4396 \\ 0.9039 & -0.4244 & 0.0527 \\ 0.1443 & 0.4186 & 0.8966 \end{pmatrix}$$

$$\mathbf{U}_2 = \begin{pmatrix} -0.5493 & -0.1939 & -0.8129 \\ 0.8274 & -0.2622 & -0.4966 \\ -0.1169 & -0.9453 & 0.3044 \end{pmatrix}$$

$$\mathbf{U}_3 = \begin{pmatrix} -0.2528 & -0.9594 & 0.1251 \\ 0.8382 & -0.1526 & 0.5236 \\ -0.4832 & 0.2373 & 0.8428 \end{pmatrix}$$

The core tensor of the Tucker 3 then follows from the application of Eq. (8). Its unfolding $\mathbf{G}_{(1)}$ is equal to the matrix as as shown at the bottom of this page.

From the core tensor, it is true that $|g_{111}| = \max\{|g_{i_1 i_2 i_3}| \mid 1 \le i_n \le 3\}$.

According to *Theorem* 1, we can define the relative perturbation ratio $\gamma = \frac{|\delta g|}{|g_{i_1 i_2 \cdots i_p}|}$ to measure the variation between the original tensors, where $|\delta g|$ denotes the disturbance intensity. Under the condition that $|\delta g|$ is fixed, the relative disturbance rate γ depends on the value of $|g_{i_1 i_2 \cdots i_p}|$. When $|g_{i_1 i_2 \cdots i_p}|$ takes the maximum, the relative perturbation rate γ is the minimum. Therefore, here, we consider embedding the watermark information at $g_{11\cdots1}$ of the core tensor, which makes the minimum change.

III. PROPOSED TENSOR DOMAIN-BASED COLOR IMAGE WATERMARKING

In this section, a new color image watermarking method based on the tensor domain is proposed. First, in order to preserve the intrinsic structure of the pixels in color images, color images are regarded as tensors. Second, the original color image space is transformed into the core tensor domain by the Tucker decomposition. Finally, according to the above theoretical analyses, the watermark is embedded into the color image in the tensor domain, and the watermark information can also be extracted accurately. Then, the processes of the watermark embedding and extraction are discussed as follows.

A. WATERMARKING EMBEDDING PROCEDURE

Let us consider an original color image $\mathbf{I}$ as a host image with the size of $M \times M \times 3$ and an $N \times N$ watermark $\mathbf{W}$. Generally, the size of the watermark should be smaller than the size of the host image. It is noted that the innovation of this paper is not how the embedded information is selected. In fact, we can choose other watermarks for embedding. The key to this paper is how to explore the new space in the color image as the embedding position of the watermark. Here, the integrity of the color image is considered, the host color image is divided, and the three channels are considered to have integrity. The color image block is regarded as the third order tensor, which can effectively keep the internal structure information between the color image pixels but also be conducive to the watermark embedding and extraction. Then, using the tensor decomposition, the core tensor and the three projection matrices in each direction are obtained. We analyze the properties of the core tensor and determine the watermark embedding position. The proposed watermark embedding method is shown in Fig. 1.

Step 1: To enhance the security of the proposed method and eliminate the spatial correlation between the pixels of the binary watermark, the watermark is scrambled from $\mathbf{W}$ to $\mathbf{W}'$ at first with the Arnold transform, which is defined as follows [30]:

$$\begin{pmatrix} x' \\ y' \end{pmatrix} = \left[\begin{pmatrix} a & b \\ c & d \end{pmatrix} \begin{pmatrix} x \\ y \end{pmatrix} + \begin{pmatrix} e \\ f \end{pmatrix} \right] \mod (l) \qquad (25)$$

where (x, y) and (x', y') are the coordinates of the original watermark pix $\mathbf{W}$ and the scrambled watermark pixel $\mathbf{W}'$, respectively. Here, we set $a = 1, b = 1, c = 1, d = 2$, $e = 0$ and $f = 0$. We perform the Arnold transform k times. k is saved as a key and used in the watermark extraction procedure.

Step 2: Divide the host color image $\mathbf{I}$ *into* $m \times m \times 3$ non-overlapping blocks. Thus, the size of the image block is $m \times m \times 3$, $m = \lfloor \frac{M}{N} \rfloor$. To preserve the integrity of the RGB

$$\begin{pmatrix} 0.7394 & -2.1384 & -1.0722 & 1.4367 & -1.2078 & 1.3790 & -0.2725 & 0.7015 & -0.8236 \\ 1.7119 & -0.8396 & 0.9610 & -1.9609 & 2.9080 & -1.0582 & 1.0984 & -2.0518 & -1.5771 \\ -0.1941 & 1.3546 & 0.1240 & -0.1977 & 0.8252 & -0.4686 & -0.2779 & -0.3538 & 0.5080 \end{pmatrix}$$

$$\begin{pmatrix} \mathbf{4.7388} & 0.6782 & 0.1015 & -0.6205 & 1.6449 & 0.7119 & 0.1923 & 1.5070 & -0.2464 \\ -0.4795 & 1.6428 & -0.3034 & -2.8012 & 0.3901 & 0.1760 & 0.6934 & -0.8650 & 0.5908 \\ 0.0177 & -0.3261 & -0.4061 & -0.0870 & -0.1150 & 0.5276 & 0.1211 & -0.0582 & -0.0087 \end{pmatrix}$$
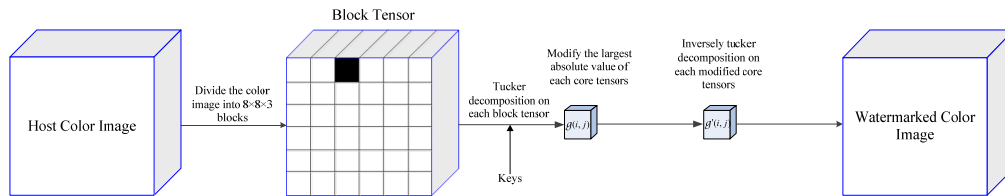
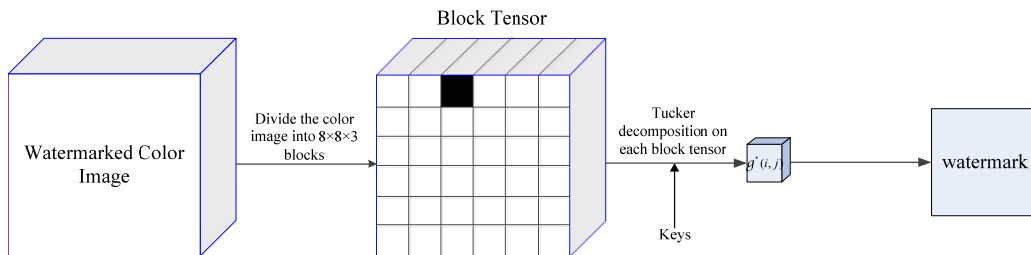**FIGURE 1.** Flowchart of the proposed watermark embedding method.

FIGURE 2. Flowchart of the proposed watermark extraction.

three channels and the spatial position relationship, each color image block is regarded as a third order tensor. It is assumed here that $\mathcal{A}(i, j)$ is defined as the color image block at the position of (i, j), where $i, j = 1, 2, \cdots, N$.

Step 3: Perform the Tucker 3 decomposition on each block.

$$\mathcal{A}(i, j) = g(i, j) \times_1 \mathbf{U}_1 \times_2 \mathbf{U}_2 \times_3 \mathbf{U}_3 \qquad (26)$$

where $g \in R^{m \times m \times 3}$ is the core tensor, and $\mathbf{U}_1 \in R^{m \times m}$, $\mathbf{U}_2 \in R^{m \times m}$ and $\mathbf{U}_3 \in R^{3 \times 3}$ are the projection matrices in the three directions of the color image, respectively. Here, we mainly analyze the property of the core tensor $g \in R^{m \times m \times 3}$. Thus, we define $g_{a\max}(i, j) = \left\{ g_{xyz} \left| \max_{x, y, z} |g_{xyz}| \right. \right\}$, and the position of $\max_{x, y, z} |g_{xyz}|$ is fixed (i.e., $x = 1, y = 1, z = 1$). Since the change of $g_{a\max}(i, j)$ is the minimal to the original core tensor, we consider embedding the watermark information into this location.

Step 4: Consider embedding the watermark $\mathbf{W}'$ into the core tensor $g \in R^{m \times m \times 3}$. Here, QIM is used to embed watermark information [31], [32]. For each block, $g_{a\max}(i, j)$ of the core tensor $g(i, j)$ is used to embed one bit of the watermark:

$$g'_{a\max}(i, j)$$

$$= \begin{cases} \text{sign}(g_{a\max}(i, j))(2T \times \text{round}(\dfrac{|g_{a\max}(i, j)|}{2T}) + \dfrac{T}{2}) \\ \qquad \text{if } \mathbf{W}'(i, j) = 1 \\ \text{sign}(g_{a\max}(i, j))(2T \times round(\dfrac{|g_{a\max}(i, j)|}{2T}) - \dfrac{T}{2}) \\ \qquad \text{if } \mathbf{W}'(i, j) = 0 \end{cases}$$

$$(27)$$

where $\text{sign}(\cdot)$ represents the sign function, T is the quantization step controlling the embedding strength of the watermark bit, $\text{round}(\cdot)$ denotes the rounding operation to the nearest integer, and $\mathbf{W}'$ denotes the scrambled watermark bit at the position of (i, j).

According to Eq. (27), the original core tensor $g(i, j)$ is modified to $g'(i, j)$. It should be emphasized that the main innovation of this paper is to embed the watermark information in the tensor domain. That is, we can use other embedded watermarking approaches in this step.

Step 5: Perform the inverse Tucker decomposition on each black at (i, j) as

$$g'(i, j) \times_1 \mathbf{U}_1 \times_2 \mathbf{U}_2 \times_3 \mathbf{U}_3 \Rightarrow \mathcal{A}'(i, j) \qquad (28)$$

Step 6: Thus, the reconstructed color image $\mathbf{I}_W$ is obtained by $\mathcal{A}'(i, j)$.

B. WATERMARKING EXTRACTION PROCEDURE

In this subsection, we will propose the watermark extraction method from a received color image $\mathbf{I}_W$. Fig. 2 shows the schematic diagram of the proposed watermark extraction scheme. The specific watermark extraction steps are described as follows:

Step 1: Divide the received color image $\mathbf{I}_W$ into $m \times m \times 3$ non-overlapping blocks. Here, $\mathcal{A}^*(i, j)$ denotes the (i, j)-th image block, and $i, j = 1, 2, \cdots, N$.

Step 2: Compute the core tensor by using the Tucker 3 decomposition:

$$\mathcal{A}^*(i, j) = g^*(i, j) \times_1 \mathbf{U}_1^* \times_2 \mathbf{U}_2^* \times_3 \mathbf{U}_3^* \qquad (29)$$

FIGURE 3. Ten test original color images with the size of 512×512: from (a) to (j), and two watermarks with a size of 64×64: (k) and (l).
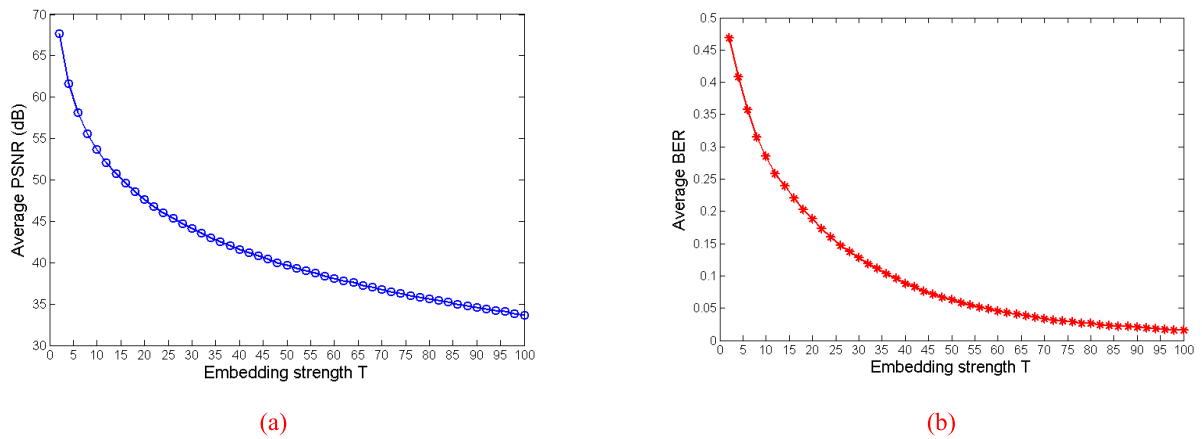

(a)

(b)

FIGURE 4. Selection of the Quantization Step T: (a) Average PSNR values obtained over ten original color images and two watermarks depending on the embedding strength. (b) Average BER value obtained over ten original color images and two watermarks depending on the embedding strength.

where $g^* \in R^{m \times m \times 3}$ is the core tensor and $g_{a\,\max}^*(i,j)$ denotes position (1,1,1) of the core tensor $g^*(i,j)$.

Step 3: For the core tensor $g^*(i,j)$ of each color image block, a one-bit watermark at the position of (i,j), $w_1^*(i,j)$, is extracted by using the following equation:

$$w_1^*(i,j) = \arg_{\theta \in \{0,1\}} \min \left| \left| g_{a\,\max}^{(\theta)}(i,j) \right| - \left| g_{a\,\max}^*(i,j) \right| \right| \quad (30)$$

where $g_{a\,\max}^{(\theta)}(i,j)$ is represented as follows:

$$g_{a\,\max}^{(\theta)}(i,j)$$

$$= \begin{cases} \text{sign}(g_{a\,\max}^*(i,j)) \cdot (2T \times \text{round}(\dfrac{|g_{a\,\max}^*(i,j)|}{2T}) + \dfrac{T}{2}) \\ \quad \text{if } \theta = 1 \\[2mm] \text{sign}(g_{a\,\max}^*(i,j)) \cdot (2T \times \text{round}(\dfrac{|g_{a\,\max}^*(i,j)|}{2T}) - \dfrac{T}{2}) \\ \quad \text{if } \theta = 0 \end{cases}$$

(31)

Step 4: Perform the inverse Arnold transform on $\mathbf{W}_1^*$ to obtain the extracted watermark information $\mathbf{W}^*$.

IV. EXPERIMENTAL RESULTS

In this section, several experiments have been carried out to examine the robustness and imperceptibility of the proposed color image watermarking method based on the tensor domain for image copyright protection. To conduct these experiments, 10 color images with a size of 512×512 from the IVY image database [33] are considered, and two binary images with the size of 64×64 from the MPEG-7 database [34] are used as watermarks in the experiments. That is, 4096 bits are embedded into each host color image and a one bit watermark is embedded into each block of the host color image. The host color images and watermarks are shown in Fig. 3.

To evaluate the imperceptibility of the watermarked color image, we first define the single channel PSNR$_i$ as follows:

$$\text{PSNR}_i = 10 \log_{10} \frac{255^2}{\text{MSE}_i} \quad (32)$$

PSNR=38.84	PSNR=39.88	PSNR=38.71	PSNR=39.19	PSNR=39.53
BER=0	BER=0	BER=0	BER=0	BER=0
PSNR=38.92	PSNR=39.72	PSNR=39.08	PSNR=39.09	PSNR=38.99
BER=0	BER=0	BER=0	BER=0	BER=0
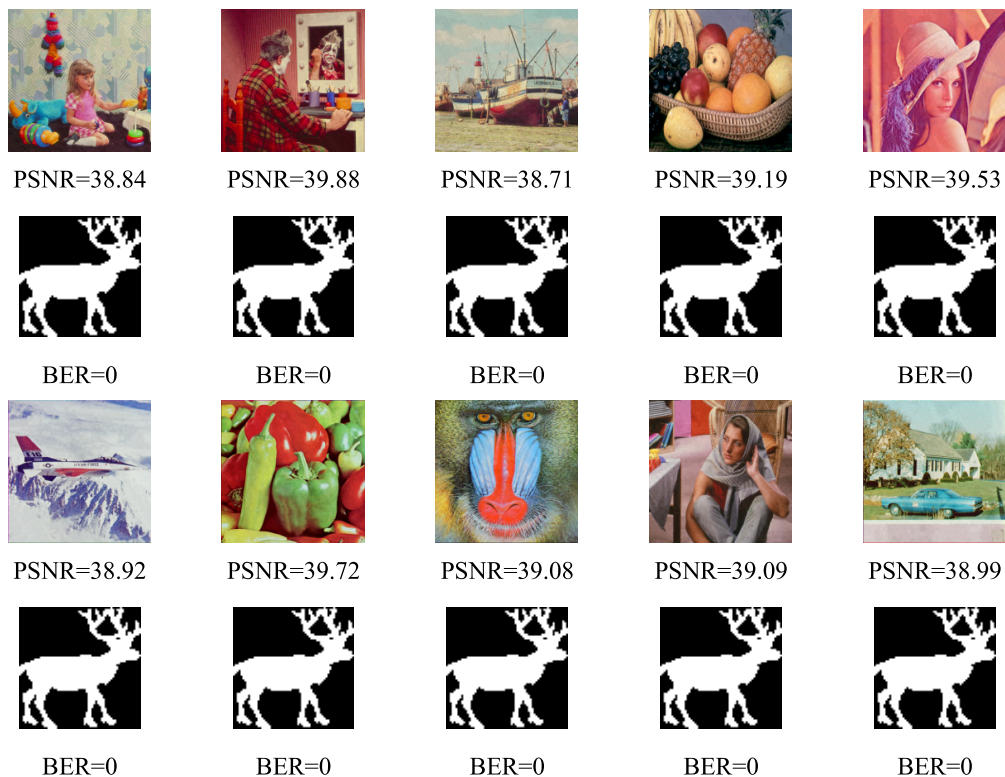
FIGURE 5. The results of embedding and extracting watermarks without any attacks.

TABLE 1. Attacks and attack strength.

Attack type	Strength
Median filter	Kernel size: 3×3, 5×5, 7×7
Average filter	Kernel size: 3×3, 5×5, 7×7
Gaussian noise	Variance: 0.01, 0.02, 0.03
Salt and pepper noise	Density: 0.01, 0.02, 0.03
JPEG compression	Compression quality: 90, 80, 70
Gaussian blur	Standard derivation: 0.5, 1, 1.5
Motion blur	Pixels 45◦ : 5, 10, 15
Image sharpening	Radius: 1, 2, 3
Scaling	Scaling factor: 0.9, 1.1, 1.2
Rotation	Rotation angle: 25◦ , 50◦ , 75◦
Removing the upper rows	Row numbers: 50, 100, 150

where MSE_i is mean square error of the i-th channel, which is given by

$$\text{MSE}_i = \frac{1}{M \times M} \sum_{x=0}^{M-1} \sum_{y=0}^{M-1} (I(x, y, i) - I_W(x, y, i))^2 \quad (33)$$

Thus, the PSNR of the color image is defined according to Eq. (32):

$$\text{PSNR} = \frac{1}{3} \sum_{i=1}^{3} \text{PSNR}_i \quad (34)$$

TABLE 2. Some examples of extracted watermarks and their BER values under different attacks.

	Average filter 5×5	Median filter 5×5	Gaussian noise 0.01	Salt and pepper noise	JPEG compression	Gaussian blur
T= 50	BER=0.0945	BER=0.0122	BER=0.1912	BER=0.2532	BER=0.2021	BER=0.0557
T= 80	BER=0.0754	BER=0.0027	BER=0.0867	BER=0.0945	BER=0.0342	BER=0.0610

	Motion blur	Image sharpening	Scaling 110	Rotation 50	Cropping the upper rows 100
T= 50	BER= 0.1030	BER=0.0286	BER=0.1257	BER=0.0884	BER=0.0767
T= 80	BER= 0.0784	BER=0.0054	BER=0.0774	BER=0.0837	BER=0.0781

In addition, to evaluate the performance in terms of the watermark's robustness, the bit error rate (BER) and normalized correlation (NC) are defined as follows:

$$\text{BER} = \frac{\sum_{i=1}^{N}\sum_{j=1}^{N}|w^*(i,j) - w(i,j)|}{N \times N} \quad (35)$$

$$NC = \frac{\sum_{i=1}^{N}\sum_{j=1}^{N}(w(i,j) \cdot w^*(i,j))}{\sqrt{\sum_{i=1}^{N}\sum_{j=1}^{N}(w(i,j))^2}\sqrt{\sum_{i=1}^{N}\sum_{j=1}^{N}(w^*(i,j))^2}} \quad (36)$$

A. SELECTION OF THE QUANTIZATION STEP T

For the proposed color image watermarking method, it is necessary to determine the proper quantization step for the watermark embedding. In this section, we discuss the relationship between the quantization step T and the PSNR of the watermarked color image in order to select the proper

T in the proposed method. Here, 10 original color images and two watermarks are used. The quantization step T is increasing from 2 to 100 with an increment equal to 2. Then, the PSNR value of the watermarked color image is calculated. Fig. 4 (a) shows the average PSNR values of the watermarked images with these different quantization steps. It can be found from Fig. 4 (a) that the PSNR value of the watermarked color images decreases with the increase in the quantization step. In addition to considering the average PSNR, the robustness of the watermarking is also tested. Fig. 4 (b) shows the relationship between the quantization step T and the average BER value. It is found from Fig. 4 (b) that the average BER decreases monotonically with the increase of the quantization step T. When the smaller quantization step is taken, the larger BER value is created too, which indicates that the smaller quantization step reduces the robustness of the proposed color image watermarking method. To make the watermark imperceptible, we consider the average PSNR between 35 dB and 40 dB. Here, we set $T = 50$ and $T = 80$.

TABLE 3. Some examples of extracted watermarks and their BER values under average filter attacks.

Attack types	Strength	Extracted watermarks	BER	Extracted watermarks	BER
R-attack Average filter	3×3		0.0283		0.0291
	5×5		0.0813		0.0798
	7×7		0.1177		0.1157
G-attack Average filter	3×3		0.0200		0.0193
	5×5		0.0583		0.0588
	7×7		0.1050		0.1033
B-attack Average filter	3×3		0.0007		0.0010
	5×5		0.0115		0.0115
	7×7		0.0327		0.0330

B. INVISIBILITY TEST

Fig. 5 shows the visual quality of the watermarked color images and the extracted watermark information without an attack. In this experiment, we set the quantization step as $T = 50$. It can be seen from Fig. 5 that the PSNR values of the 10 test images is approximately 39 when the watermark is embedded, which ensures that the visual quality of the color image is imperceptible after the watermark is embedded.

TABLE 4. Some examples of extracted watermarks and their BER values under median filter attacks.

Attack types	Strength	Extracted watermarks	BER	Extracted watermarks	BER
R-attack Median filter	3×3		0		0
	5×5		0.0027		0.0027
	7×7		0.0208		0.0195
G-attack Median filter	3×3		0		0
	5×5		0.0017		0.0015
	7×7		0.0154		0.0149
B-attack Median filter	3×3		0		0
	5×5		0.0046		0.0049
	7×7		0.0198		0.0188

In addition, Fig. 5 also shows that the watermark extraction BER=0 without attack, which ensures the integrity of the watermark.

C. ROBUSTNESS TEST

To test the robustness of the proposed color image watermarking method, we use different attack types and attack strengths.

TABLE 5. NC values for some attacks.

Attack types	Spatial domain [21]	DCT-domain [35]	DWT-domain [36]	QDFT-domain [26]	Proposed
Salt and pepper noise (0.01)	0.7488	0.8239	0.8758	0.8954	**0.9186**
Gaussian noise (0.005)	0.6005	0.7310	0.8301	0.8413	**0.8704**
Median filter (3×3)	0.9408	0.8507	0.8275	0.7507	**0.9831**
Average filter (3×3)	0.9245	0.7956	0.7832	0.7956	**0.9426**
Gaussian filter (3×3)	**0.9342**	0.8112	0.8022	0.8364	0.8514
JPEG compression (80)	**0.9999**	**0.9999**	0.9143	0.9331	0.8538
Cropping 1/3	0.6134	0.7754	0.5738	0.8036	**0.8570**
Cropping 1/2	0.4519	0.6266	0.4303	0.6523	**0.7032**
Scale 0.9	0.9457	0.9917	0.9045	**1.0000**	0.9334

Table 1 shows the attack types and attack strengths, which included the most common image processing and geometric attacks. Each watermarked image is distorted by considering various attacks. Table 2 shows the Lena image as an example to extract the results of watermarks and their corresponding BER values under different attacks. It can also be found from Table 2 that the proposed color image watermarking method has good robustness to the different attacks, and it has strong anti-interference ability to Median filter and Image sharpening attacks. Relative to Gaussian noise and Salt and Pepper noise attacks, it is less robust.

Since color images have the three R, G, and B channels, we consider R-attacks, G-attacks and B-attacks for the Average filter and Median filter, respectively. Table 3 and Table 4 show the impacts of different color channel attacks on watermark extraction. From Table 3 and Table 4, it is found that the R-attack has the greatest impact on watermark extraction under the same attack strength, followed by the G-attack and B-attack. It also shows that modifying the core tensor has a slightly smaller effect on the G and B channels.

Fig. 6 shows the mean BER values for the 10 original color images and 2 watermarks under different attack types and strengths. It can be observed from Fig. 6 that (1) the BER values increase with the enhancement of the attack strength, and (2) by increasing the quantization strength T from 50 to 80, the proposed color image watermarking is robust to different attacks.

D. COMPARISON WITH SOME COLOR IMAGE WATERMARKING METHODS

To further illustrate the performance of the proposed color image watermarking method, we compare the proposed method with current, state-of art color image watermarking methods, including the spatial domain-based method [21], the DCT-domain-based method [35], the DWT-domain-based method [36] and the QDFT-domain-based method [26]. The spatial domain-based method, the DCT-domain-based method and the DWT-domain-based method worked with the YCrCb brightness component, which is also called the Y-component. For the
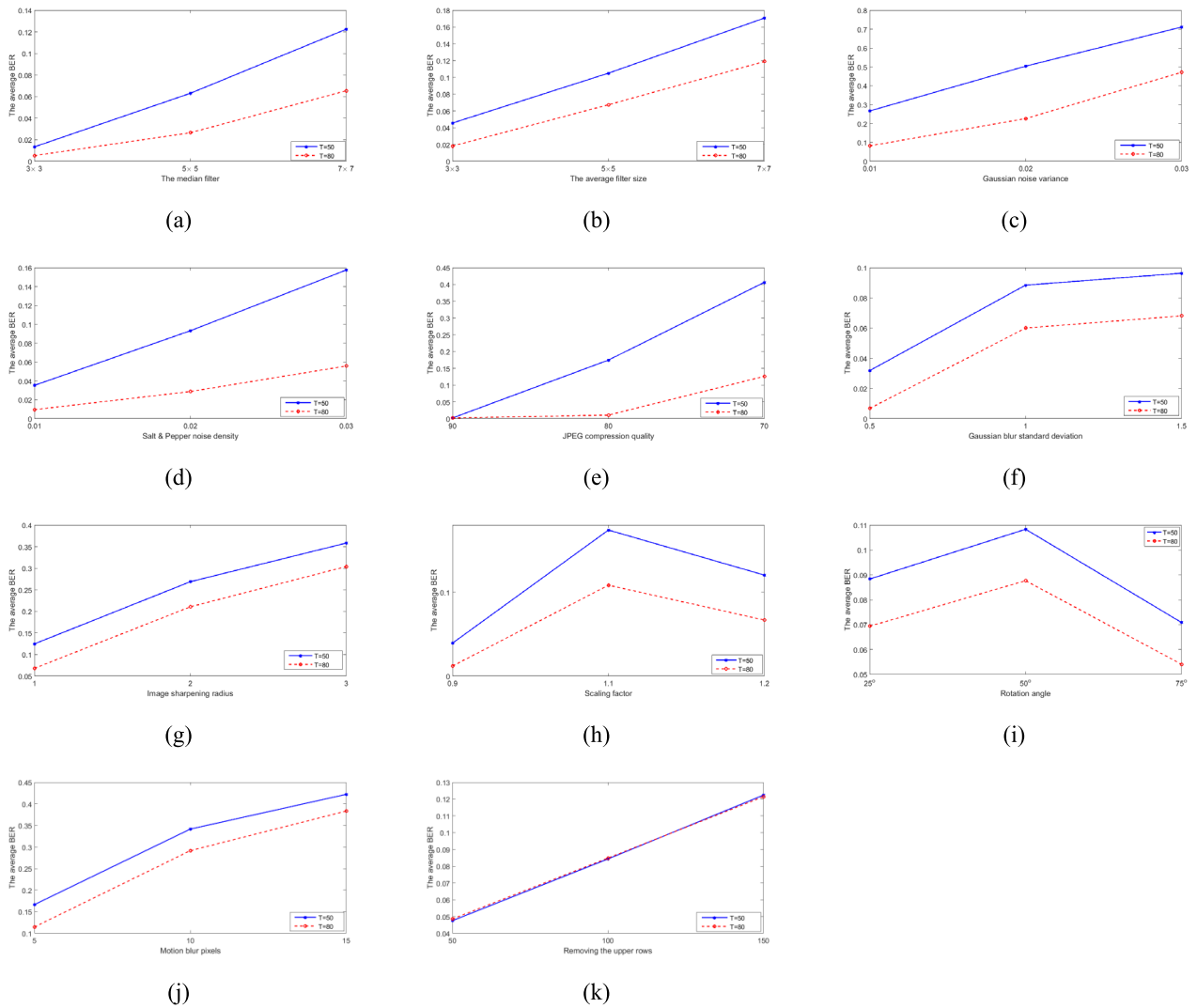
FIGURE 6. The average BER values of the color image watermarking based on the tensor domain under different attacks.

QDFT method, the watermark information is embedded into the j imaginary part. For a fair comparison, the PSNR values of all watermarked images are controlled at 40 dB by adaptively adjusting the embedding strength for all the methods. Table 5 shows the NC values.

It can be seen form Table 5 that although the spatial domain-based method achieves good results on the filtering operations (i.e., median filter, average filter, and Gaussian filter) and JPEG compression, it fails to resist noise attacks and cropping attacks. It is not the same case for transformation domain-based methods. The DCT domain-based method obtains good results on JPEG compression and scale attacks, but it cannot achieve satisfactory results in other attack types, and the QDFT-domain-based method has achieved good results in noise attacks, cropping attacks and scale attacks. Compared with other methods, the proposed method in noise attacks, filtering attacks, and cropping attacks has achieved good results. In the Salt and pepper noise, Gaussian noise,

Media filter, Gaussian filter and Cropping it has achieved the best results. However, the proposed method cannot achieve good results under JPEG compression. The reason for this is that the proposed method modifies all three RGB channels, which may lead to poor performance on JPEG Compression. In short, compared with other methods, the proposed method is robust to all kinds of attacks.

V. CONCLUSION
In this paper, a robust blind color image watermarking based on the tensor domain is proposed. The main technical contribution of the proposed method is that different from the general image watermarking methods, a new watermarking method based on tensor domain is explored, and theoretical analyses and mathematical proofs are given. The color image is regarded as a tensor, and the tensor decomposition is used to obtain the core tensor. The watermark is embedded into the core tensor by modifying the value of the optimal

embedding position. Finally, the watermark is spread to the three channels of the color image through inverse tensor decomposition. The experimental results show that the proposed method is robust to various attacks. Since the three channels of the RGB color image are considered as a whole, we can also view video as a tensor. In the future, we will study the video watermarking method based on the tensor domain.

REFERENCES

[1] Q. Jiang, F. Shao, W. Lin, and G. Jiang, "Learning sparse representation for objective image retargeting quality assessment," *IEEE Trans. Cybern.*, vol. 48, no. 4, pp. 1276–1289, Apr. 2018.

[2] Q. Jiang, F. Shao, W. Lin, K. Gu, G. Jiang, and H. Sun, "Optimizing multistage discriminative dictionaries for blind image quality assessment," *IEEE Trans. Multimedia*, vol. 20, no. 8, pp. 2035–2048, Aug. 2018.

[3] C.-S. Chang and J.-J. Shen, "Features classification forest: A novel development that is adaptable to robust blind watermarking techniques," *IEEE Trans. Image Process.*, vol. 26, no. 8, pp. 3921–3935, Aug. 2017.

[4] Y. Erfani, R. Pichevar, and J. Rouat, "Audio watermarking using spikegram and a two-dictionary approach," *IEEE Trans. Inf. Forensics Security*, vol. 12, no. 4, pp. 840–852, Apr. 2017.

[5] J. Zhang and L. Liu, "Publicly verifiable watermarking for intellectual property protection in FPGA design," *IEEE Trans. Very Large Scale Integr. (VLSI) Syst.*, vol. 25, no. 4, pp. 1520–1527, Apr. 2017.

[6] X. Liu, G. Han, J. Wu, Z. Shao, G. Coatrieux, and H. Shu, "Fractional Krawtchouk transform with an application to image watermarking," *IEEE Trans. Signal Process.*, vol. 65, no. 7, pp. 1894–1908, Apr. 2017.

[7] J. Zhang, Y. Lin, Q. Wu, and W. Che, "Watermarking FPGA bitfile for intellectual property protection," *Radioengineering*, vol. 21, no. 2, pp. 764–771, 2012.

[8] J. Zhang, Y. Lin, W. Che, Q. Wu, Y. Lu, and K. Zhao, "Efficient verification of IP watermarks in FPGA designs through lookup table content extracting," *IEICE Electron. Express*, vol. 9, no. 22, pp. 1735–1741, 2012.

[9] D. Bhowmik and C. Abhayaratne, "Quality scalability aware watermarking for visual content," *IEEE Trans. Image Process.*, vol. 25, no. 11, pp. 5158–5172, Nov. 2016.

[10] T. Zong, Y. G. Xiang, S. Guo, and Y. Rong, "Rank-based image watermarking method with high embedding capacity and robustness," *IEEE Access*, vol. 4, pp. 1689–1699, 2016.

[11] C.-K. Chan and L. M. Cheng, "Hiding data in images by simple LSB substitution," *Pattern Recognit.*, vol. 37, no. 3, pp. 469–474, Mar. 2004.

[12] I. Nasir, Y. Weng, J. Jiang, and S. Ipson, "Multiple spatial watermarking technique in color images," *Signal Image Video Process.*, vol. 4, no. 2, pp. 145–154, 2010.

[13] I. Usman and A. Khan, "BCH coding and intelligent watermark embedding: Employing both frequency and strength selection," *Appl. Soft Comput.*, vol. 10, no. 1, pp. 332–343, Jan. 2010.

[14] E. Vahedi, R. A. Zoroofi, and M. Shiva, "Toward a new wavelet-based watermarking approach for color images using bio-inspired optimization principles," *Digit. Signal Process.*, vol. 22, no. 1, pp. 153–162, Jan. 2012.

[15] X. He, C. Zhu, and Q. Wang, "The blind watermarking model of the vector geospatial data based on DFT of QIM," in *Proc. IEEE Int. Conf. Netw. Infrastruct. Digit. Content*, Nov. 2009, pp. 1039–1044.

[16] A. Piva, F. Bartolinin, V. Cappellini, and M. Barni, "Exploiting the cross-correlation of rgb-channels for robust watermarking of color images," in *Proc. Int. Conf. Image Process.*, Kobe, Japan, vol. 1, Oct. 1999, pp. 306–310.

[17] N. Ahmidi and R. Safabakhsh, "A novel DCT-based approach for secure color image watermarking," in *Proc. Int. Conf. Inf. Technol., Coding Comput.*, vol. 2, Apr. 2004, pp. 709–713.

[18] C. I. Podilchuk and W. Zeng, "Image-adaptive watermarking using visual models," *IEEE J. Sel. Areas Commun.*, vol. 16, no. 4, pp. 525–539, May 1998.

[19] N. Kaewamnerd and K. R. Rao, "Wavelet based image adaptive watermarking scheme," *Electron. Lett.*, vol. 36, no. 4, pp. 312–313, 2000.

[20] M. Barni, F. Bartolini, and A. Piva, "Multichannel watermarking of color images," *IEEE Trans. Circuits Syst. Video Technol.*, vol. 12, no. 3, pp. 142–156, Mar. 2002.

[21] Q. Su, Y. Niu, Q. Wang, and G. Sheng, "A blind color image watermarking based on DC component in the spatial domain," *Optik-Int. J. Light Electron Opt.*, vol. 124, no. 23, pp. 6255–6260, Dec. 2013.

[22] H. M. Al-Otum and N. A. Samara, "A robust blind color image watermarking based on wavelet-tree bit host difference selection," *Signal Process.*, vol. 90, no. 8, pp. 2498–2512, 2010.

[23] C.-H. Chou and K.-C. Liu, "A perceptually tuned watermarking scheme for color images," *IEEE Trans. Image Process.*, vol. 19, no. 11, pp. 2966–2982, Nov. 2010.

[24] T. K. Tsui, X.-P. Zhang, D. Androutsos, "Color image watermarking using the spatio-chromatic Fourier transform," in *Proc. IEEE ICASSP*, May 2006, p. 2.

[25] T. K. Tsui, X.-P. Zhang, and D. Androutsos, "Color image watermarking using multidimensional Fourier transforms," *IEEE Trans. Inf. Forensic Security*, vol. 3, no. 1, pp. 16–28, Mar. 2008.

[26] B. Chen, G. Coatrieux, G. Chen, X. Sun, J. L. Coatrieux, and H. Z. Shu, "Full 4-D quaternion discrete Fourier transform based watermarking for color images," *Digit. Signal Process.*, vol. 28, no. 1, pp. 106–119, 2014.

[27] J. Ouyang, G. Coatrieux, B. Chen, and H. Shu, "Color image watermarking based on quaternion Fourier transform and improved uniform log-polar mapping," *Comput. Elect. Eng.*, vol. 46, pp. 419–432, Aug. 2015.

[28] R. E. Bellman, *Matrix Analysis*. New York, NY, USA: McGraw-Hill, 1978.

[29] P. A. Regalia and S. K. Mitra, "Kronecker products, unitary matrices and signal processing applications," *SIAM Rev.*, vol. 31, no. 4, pp. 586–613, 1989.

[30] Z. Liu *et al.*, "Color image encryption by using Arnold transform and color-blend operation in discrete cosine transform domains," *Opt. Commun.*, vol. 284, no. 1, pp. 123–128, 2011.

[31] B. Chen and G. W. Wornell, "Quantization index modulation: A class of provably good methods for digital watermarking and information embedding," *IEEE Trans. Inf. Theory*, vol. 47, no. 4, pp. 1423–1443, May 2001.

[32] H.-Y. Yang, X.-Y. Wang, P.-P. Niu, and A.-L. Wang, "Robust color image watermarking using geometric invariant quaternion polar harmonic transform," *ACM Trans. Multimedia Comput. Commun.*, vol. 11, no. 3, 2015, Art. no. 40.

[33] P. L. Callet and F. Autrusseau. (2005). *Subjective Quality Assessment IRCCyN/IVC Database*. [Online]. Available: http://www.irccyn.ec-nantes.fr/ivcdb/

[34] R. Ralph. (1999). *MPEG-7 Core Experiment CE-Shape-1*. [Online]. Available: http://www.dabi.temple.edu/~shape/MPEG7/dataset.html

[35] C. Das, S. Panigrahi, V. K. Sharma, and K. K. Mahapatra, "A novel blind robust image watermarking in DCT domain using inter-block coefficient correlation," *AEU-Int. J. Electron. Commun.*, vol. 68, no. 3, pp. 244–253, 2014.

[36] L. P. Feng, L. B. Zheng, P. Cao, "A DWT-DCT based blind watermarking algorithm for copyright protection," in *Proc. IEEE ICCIST*, Jul. 2010, pp. 455–458.
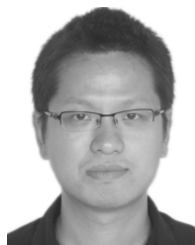
HAIYONG XU is currently pursuing the Ph.D. degree with the Faculty of Information Science and Engineering, Ningbo University. He is currently a Teacher with the College of Science and Technology, Ningbo University. His research interests include multimedia communication, image processing, and machine learning.

GANGYI JIANG received the M.S. degree from Hangzhou University in 1992 and the Ph.D. degree from Ajou University, South Korea, in 2000. He is currently a Professor with the Faculty of Information Science and Engineering, Ningbo University, China. His research interests mainly include image/video processing, video coding, and visual perception. He has authored over 100 technical articles in refereed journals.

MEI YU received the B.S. and M.S. degrees from the Hangzhou Institute of Electronics Engineering, China, in 1990 and 1993, and the Ph.D. degree from Ajou University, South Korea, in 2000. She is currently a Professor with the Faculty of Information Science and Engineering, Ningbo University, China. Her research interests mainly include image/video coding and visual perception.

TING LUO is currently pursuing the Ph.D. degree with the Faculty of Information Science and Engineering, Ningbo University. He is currently a Teacher with the College of Science and Technology, Ningbo University. His research interests include multimedia security, image processing, data hiding, and pattern recognition.

• • •